Arabian Journal of Chemistry (2022) **15**, 103587

King Saud University

Arabian Journal of Chemistry

www.ksu.edu.sa
www.sciencedirect.com

ORIGINAL ARTICLE

Synthesis of an advanced Pd-Rh bimetallic catalyst for gasoline engine emission control

Li Lan [a], Shanhu Chen [b,*], Suning Wang [c], Junhuai Xiang [a], Long Huang [a], Meihua Zhu [b], Huasheng Lin [b]

[a] *College of Materials and Mechatronics, Jiangxi Science and Technology Normal University, Nanchang 330013, China*
[b] *College of Chemistry and Chemical Engineering, Jiangxi Science and Technology Normal University, Nanchang 330013, China*
[c] *Guangxi Key Laboratory of Optical and Electronic Materials and Devices, College of Materials Science and Engineering, Guilin University of Technology, Guilin 541004, China*

Received 28 September 2021; accepted 21 November 2021
Available online 26 November 2021

KEYWORDS

Pd-Rh bimetallic catalyst;
Adjusting the synthesis procedure;
Dispersion;
Oxidation state;
Catalytic conversions

Abstract In recent years, the dramatic increase of the prices of Pd and Rh brings about increasingly heavier cost pressure for the exhaust gas after-treatment industry, thus it is of great significance to develop advanced Pd-Rh bimetallic catalysts with low metal loading. In this work, on the basis of conventional catalyst composed of Al_2O_3-supported Pd and CZ (ceria-zirconia-based oxide)-supported Rh, an advanced Pd-Rh catalyst was obtained by adjusting the synthesis procedure. That was, a small portion of Rh was co-impregnated with Pd on Al_2O_3, while the other portion was still supported on CZ. In this way, the co-impregnated Rh may act as an auxiliary for Pd/Al_2O_3 component. As revealed by the various characterization results, the agglomeration of Pd species is well suppressed, and larger amount of PdO species is maintained for the modified catalyst after hydrothermal aging treatment. On the other hand, the state of Rh species also appears to be somewhat modified. Consequently, after hydrothermal aging treatment, the modified catalyst behaves much better for the catalytic conversions of CO, HC and NO.

1. Introduction

As we all know, platinum group metals (Pt, Pd, Rh) are the most commonly used active components in the supported catalysts for gasoline engine emission control (Lan et al., 2018; Zhan et al., 2014). In practical operation of three-way catalysts (TWCs), Pd is usually applied owing to its prominent oxidation activity of CO/HC and excellent high-temperature thermal stability, and Rh is often included on account of its outstanding reduction efficiency of NO (Cao et al., 2017; Kašpar et al., 2003; Vedyagin et al., 2018). Hence, catalytic

* Corresponding author.
E-mail address: cshscu@163.com (S. Chen).
Peer review under responsibility of King Saud University.

Production and hosting by Elsevier

https://doi.org/10.1016/j.arabjc.2021.103587
1878-5352

converters consist of Pd-Rh bimetallic catalysts have been widely adopted to install near the exhaust manifold outlet of automobiles (Goto et al., 2014; Kang et al., 2014; Majumdar and Pihl, 2020; Vedyagin et al., 2017; Wu et al., 2004). However, in recent years, the prices of Pd and Rh have underwent dramatic and continuous increase, which brings about increasingly greater pressure for the exhaust gas after-treatment industry. Under this condition, it is of great significance to develop Pd-Rh bimetallic catalysts with advanced purification efficiency and low metal loading.

Generally speaking, high-surface-area Al_2O_3 and oxygen buffering component CZ are two most widely applied materials to support noble metals in TWCs (Bharali et al., 2012; Dong et al., 2012; Kašpar et al., 2003; Lan et al., 2018; Lang et al., 2017; Lin et al., 2014; Panahi-Kalamuei et al., 2015; Papavasiliou et al., 2010; Soloviev et al., 2012). In industrial application, mechanical mixture of Al_2O_3-supported Pd and CZ-supported Rh is a common combination style for Pd-Rh bimetallic catalysts (Kang et al., 2014; Kang et al., 2015). However, since the TWCs would encounter rather harsh conditions during practical operation, i.e., extremely high temperature, high space velocity, and watery atmosphere, deactivation of the catalysts would inevitably take place. Moreover, besides self-agglomeration and encapsulation by the support materials, the evolution of the chemical state of Pd and Rh species upon deactivation is different. PdO is apt to decompose at high temperature even under oxidative condition, leading to the formation of catalytically less active metallic Pd species, while Rh species has a larger tendency to transform into reduction-resistive RhO_2 species, which is highly stable and catalytically inert (Graham et al., 1999; Polvinen et al., 2004; Rassoul et al., 2001; Vedyagin et al., 2017).

As reported by numerous researchers, the Pd-Rh bimetallic catalyst systems are demonstrated to have synergistic function on both oxidation behavior of CO/HC and reduction performance of NO, and moreover, Rh is able to stabilize the particle size, the oxidation state, and consequently the activity of Pd (Fang et al., 2015; López Granados et al., 2006; Vedyagin et al., 2013). Thus, in this work, an advanced Pd-Rh bimetallic catalyst was synthesized by adjusting the synthesis procedure of conventional Pd-Rh catalyst. That was, part of Rh was co-impregnated with Pd on Al_2O_3, while the other portion was still supported on CZ. By this means, improved catalytic performance can be achieved, which is mainly ascribed to the synergistic effect of the Pd-Rh interaction.

2. Materials and methods

2.1. Synthesis of the Pd-Rh bimetallic catalysts

A conventional Pd-Rh bimetallic catalyst was prepared by mechanically mixing the impregnated catalyst powders of Al_2O_3-supported Pd and CZ-supported Rh. The support materials, i.e., γ-Al_2O_3 and CZ powders were both provided by Solvay Company. The precursors of noble metal species, Pd $(NO_3)_2$ and $Rh(NO_3)_3$ solutions (which contained some nitric acid as the stabilizer), were purchased from Shanghai Jiuyue Chemical Co. Ltd., therein the contents of $Pd(NO)_3$ and Rh $(NO)_3$ were 0.42 and 0.54 mol/L, respectively, and correspondingly, the concentrations of Pd and Rh in the salt solutions were 15 wt% and 8.11 wt%, respectively. The detailed synthesis procedure was as follows: firstly, 1.07 g of $Pd(NO_3)_2$ solution was diluted to 7.96 mL by distilled water, and then 8.0 g of γ-Al_2O_3 powders was introduced, after evenly stirring at room temperature (ca. 30 °C) for 20 min, the impregnated mixture was subsequently dried at 100 °C for 5 h and calcined at 550 °C for 3 h. In this way, Pd/Al_2O_3 powders were obtained. On the other hand, Rh/CZ powders were prepared in the same way, except that the raw materials were changed to 0.99 g of $Rh(NO_3)_3$ solution (which was diluted to 4.57 mL prior to the impregnation process) and 8.0 g of CZ powders. After that the catalyst powders of Pd/Al_2O_3 and Rh/CZ were physically mixed and blended thoroughly to get the expected Pd-Rh bimetallic catalyst, in which the theoretical loading contents of Pd and Rh were 1.0 wt% and 0.5 wt%, respectively, and this sample was hereafter named as Pd + Rh.

A modified Pd-Rh bimetallic catalyst was prepared by adjusting the synthesis procedure of the conventional Pd + Rh catalyst. That was, the precursor of Rh was divided into two portions, wherein a portion was co-impregnated with the precursor of Pd onto Al_2O_3, and the other portion was still loaded onto CZ powders. To be more specific, 1.07 g of Pd $(NO_3)_2$ solution and 0.20 g of $Rh(NO_3)_3$ solution were firstly blended together and diluted to 7.96 mL, which was then co-impregnated onto 8.0 g of γ-Al_2O_3 powders to obtain PdRh/Al_2O_3 powders, and the residual 0.79 g of $Rh(NO_3)_3$ solution was impregnated on CZ powders. After drying and calcining treatment, the PdRh/Al_2O_3 and Rh/CZ components were also mechanically mixed thoroughly, and eventually a modified catalyst labeled as PdRh + Rh was obtained.

In addition, for the purpose of evaluating the catalytic performance, 10.0 g of the catalyst powders were introduced into 15.0 mL of distilled water, and a homogeneous slurry was obtained with the assistance of a high energy ball milling machine, wherein spherical zirconia with diameter of 9 mm was used as the grinding media. After the ball milling process, the D50 (which represented the particle size where 50% of the particles were smaller than this value) of the catalyst particles was between 5 and 10 μm. After that, the slurry was coated onto a cordierite monolith (400 cpsi, Corning, USA), followed by subsequent drying at 100 °C for 5 h and calcining at 550 °C for 3 h to get the monolithic catalysts, and the loading amount was controlled to be about 120 g/L. Furthermore, to testify the catalyst durability, the above-obtained two catalysts were submitted to hydrothermal aging in an atmosphere consisted of 10 vol% H_2O in air at 1000 °C for 10 h (corresponding to 160000 km durability process for vehicles in practical use), and the aged catalysts were henceforward marked as (Pd + Rh)a and (PdRh + Rh)a, respectively.

2.2. Characterization of the catalysts

The textural parameters of the catalysts and the blank support were determined on a Quantachrome automated surface area & pore size analyzer. The granular samples were firstly degassed under vacuum at 300 °C for 4 h, and then submitted to N_2 adsorption–desorption under liquid N_2 condition (-196 °C).

Phase identification was conducted on a Rigaku DX-2500 diffractometer equipped with Cu Kα as the radiation source.

The catalyst powders were homogeneously spread onto a quartz glass plate, which were then continuously scanned with a step size of 0.02°. In this way, XRD patterns within the 2θ range of 10-90° were collected.

Raman experiment was carried out on a Renishaw inVia reflex Raman spectrometer using an excitation wavelength of 532 nm. The spectral resolution was 1 cm^{-1} and the collected frequency range of the spectra was 100–1000 cm^{-1}.

The transmission electron microscopy (TEM) images were obtained by a ZEISS Libra 200 FE electron microscope. The powder samples were dispersed in ethanol by ultrasonic oscillation. Both TEM and HRTEM images were observed at an accelerating voltage of 200 kV.

The surface elemental information was analyzed by a British Kratos XSAM-800 X-ray photoelectron spectroscopy. Monochromatic Al Kα (1486.6 eV) was applied as the radiation. The XPS spectra of Pd 3d, Rh 3d, Ce 3d, Zr 3d, Al 2p and O 1 s core levels were recorded, and the binding energies were calibrated by fixing C 1 s at 284.8 eV.

The dispersion of Pd and Rh species on the surface of the catalysts was further investigated by CO adsorption experiment on a Nicolet 6700 Fourier Transform Infrared spectrometer (FTIR). Prior to the experiment, the catalyst powders were firstly treated in H_2 at 400 °C for 1 h. After cooling down to room temperature, the samples were stayed in N_2 for at least 30 min. Afterwards CO adsorption was proceeded, followed by sweeping in N_2 for 30 min.

Hydrogen temperature-programmed reduction (H_2-TPR) experiment was performed to estimate the reduction capability of the catalysts. The samples were placed in the bottom of a U-type quartz tube. Before the reduction process, N_2 atmosphere was passed through, then the samples were heated to 400 °C and held for 1 h. After that it was cooled down to room temperature, and a mixture of 5 vol% H_2/N_2 was passed through, meanwhile the temperature was raised at a constant heating rate of 5 °C·min^{-1}. During the reduction process, the H_2 consumption was continuously monitored by a thermal conductivity detector (TCD).

2.3. Evaluation of the three-way catalytic performance

The three-way catalytic performance in terms of conversions of CO/HC/NO was evaluated employing a fixed-bed continuous flow reactor. The reaction temperature and the composition of the gas mixture were programme controlled by temperature controllers and special mass flow controllers, respectively. The reactive gas mixture that simulated the actual exhaust gas from gasoline-engined vehicles at the so-called stoichiometric condition was composed of: CO (4600 ppm), HC (330 ppm, which contained 220 ppm of C_3H_6 and 110 ppm of C_3H_8, respectively), NO (1250 ppm), H_2 (1533 ppm), CO_2 (11%), H_2O (10%), O_2 (3600 ppm), and N_2 (balance). The gas hourly space velocity (GHSV) was fixed at 50 000 h^{-1}. The atmosphere was periodically fluctuated between rich and lean conditions. Prior to the activity test, the catalysts were pretreated under reactive gas mixture at 550 °C for 1 h. The conversions of CO/HC/NO were calculated based on the compositions of the inlet and outlet gas mixtures, which were monitored by an Antaris IGS FTIR (Thermo Fisher Scientific).

3. Results and discussion

3.1. Textural parameters of the catalysts

The textural parameters of the catalysts and the blank support, including specific surface areas, pore volumes, and mean pore radii, are summarized in Table 1. Therein it is found that the specific surface areas and pore volumes of the aged samples all become smaller compared with those of the fresh ones, indicating that sintering has occurred for all samples during hydrothermal aging process. In addition, it is well known that aging treatment often brings about elimination of smaller pores and formation of relatively larger ones, as a consequence, larger mean pore radii are obtained for the aged samples. However, it is worthwhile to notice that the two catalysts possess similar textural properties, which are also similar with the blank support, regardless of the hydrothermal aging treatment. Thus, it can be concluded that the impregnation process and the adjustment of the synthesis procedure both exert little influence on the textural property of the catalysts.

3.2. XRD and Raman characterization results

Fig. 1 presents the XRD patterns of the fresh and aged catalysts, upon which phase identification could be performed. It is seen from Fig. 1(a) that the two fresh catalysts show almost the same XRD characteristics, similar cubic CZ and γ-Al_2O_3 phases are detected, while only a slight peak identified as PdO phase is observed for the noble metal species (Fig. 1(c)). Upon hydrothermal aging treatment, particle agglomeration is testified by remarkable peak sharpening in Fig. 1(b). Additionally, from Fig. 1(d), a slight peak characteristic of metallic Pd phase is detected for conventional (Pd + Rh)a, while the peak of metallic Pd phase for (PdRh + Rh)a is invisible, implying that the reduction of PdO to metallic Pd upon hydrothermal aging treatment is somewhat inhibited for (PdRh + Rh)a, which may result in catalyst deactivation to a lesser extent.

Fig. 2 displays the Raman spectra of the fresh and aged catalysts, wherein the strong band located at around 648 cm^{-1} is ascribed to the vibration of B_{1g} mode of PdO phase. Moreover, several weak peaks are observed, which are also associated with the well-developed PdO phase (Iglesias-Juez et al., 2004). In addition, γ-Al_2O_3 and Rh/RhO_x species are not Raman active, while the Raman features of cubic CZ phase seem to be overlapped with the tanglesome peaks of PdO

Table 1 Specific surface areas (S_{BET}), pore volumes (V), and mean pore radii (R) of the fresh and aged catalysts.

Samples	S_{BET} ($m^2 \cdot g^{-1}$)	V ($ml \cdot g^{-1}$)	R (nm)
Pd + Rh	135	0.44	6.5
PdRh + Rh	144	0.47	6.5
Al_2O_3 + CZ	143	0.48	6.3
(Pd + Rh)a	83	0.36	8.8
(PdRh + Rh)a	84	0.40	9.6
(Al_2O_3 + CZ)a	81	0.39	9.4

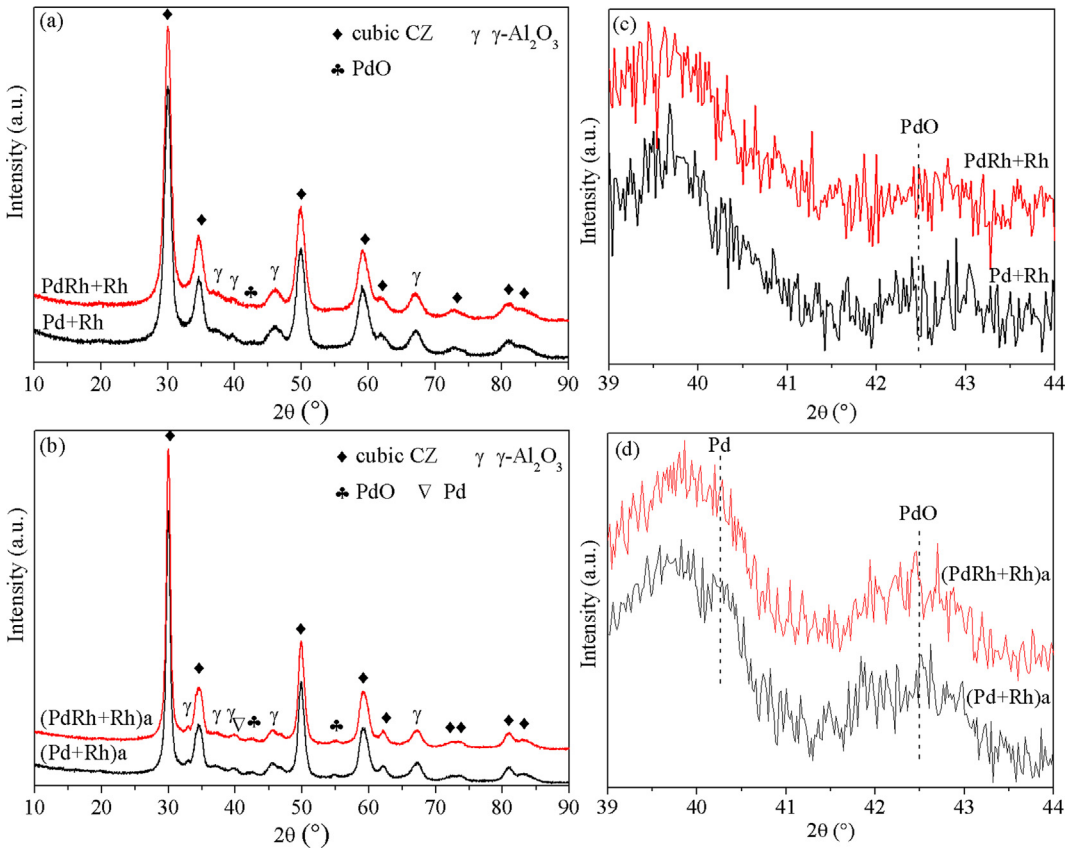

Fig. 1 XRD patterns of the fresh (a, c) and aged (b, d) catalysts.

phase, making them indistinguishable (Cao et al., 2013). Thus, it is considered that only the principal Raman peak of PdO at 648 cm^{-1} is meaningful, which can provide us some information about the oxygen state, particle size and concentration of PdO species in the catalysts (Cao et al., 2013; Graham et al., 2002). For the fresh samples, it is seen from Fig. 2(a) that the intensity of the principal Raman band of PdO for PdRh + Rh is slightly higher than that for Pd + Rh, which hints us that the co-impregnation of some Rh species with Pd is beneficial to the formation of larger amount of PdO species. After hydrothermal aging treatment, besides significant peak sharpening that is indicative of particle agglomeration, another worth noticing phenomenon is that the principal Raman band of PdO for (PdRh + Rh)a is much stronger than that for (Pd + Rh)a. This phenomenon, combining with the subsequent TEM observation that (PdRh + Rh)a possesses smaller particle size of noble metal species, tells us that (PdRh + Rh)a owns comparatively larger amount of PdO species, which is because that the co-impregnated Rh may act as an auxiliary to suppress the deactivation of Pd species.

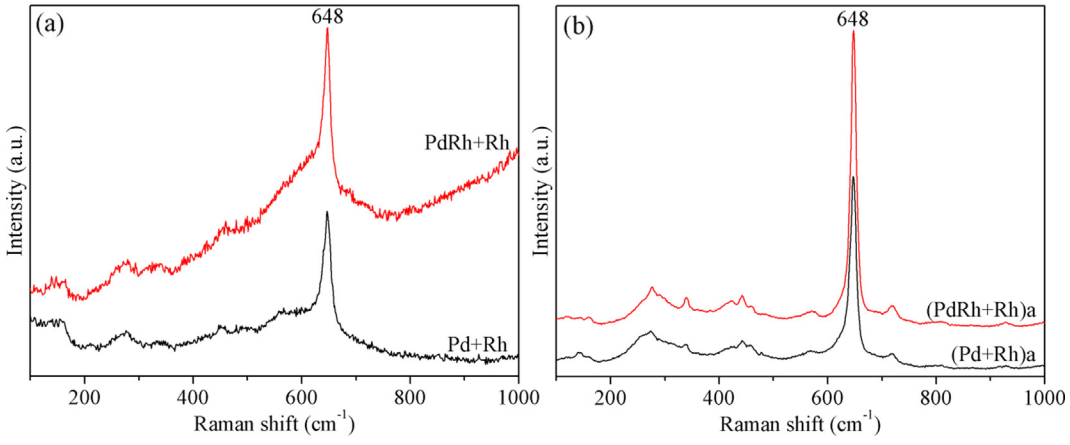

Fig. 2 Raman spectra of the fresh (a) and aged (b) catalysts.

3.3. TEM and HRTEM observations

Fig. 3 displays the TEM images of the two aged catalysts, wherein the dark particles distributed on the surface of the support materials are mainly recognized as noble metal species. For better comparison, the corresponding particle size distributions of the noble metal species (in terms of both histogram and the normality test results) are also included in Fig. 3. As seen therein, the noble metal species in (PdRh + Rh)a exhibits smaller particle size, demonstrating that the co-impregnation of partial Rh together with Pd is beneficial to maintain relatively higher dispersion of noble metal species after hydrothermal aging treatment. This phenomenon can be also proven by the HRTEM results in Fig. 4, wherein the particles are identified according to their interplanar crystal spacing measured by a special software (DigitalMicrograph). Moreover, it is worthwhile to notice from Fig. 4 that the oxidation states of the noble metals in (PdRh + Rh)a are also modified. Compared with conventional (Pd + Rh)a, which owns large metallic Pd particles and reduction-resistive RhO_2 species, more oxidative PdO and reducible Rh_2O_3 species are observed for (PdRh + Rh)a. In addition, Rh_2O_3 particles in close contact with the Al_2O_3 support are observed in Fig. 4 (b1) and 4(b3), which confirms the loading of Rh on Al_2O_3 for the modified catalyst (PdRh + Rh)a. Taking into account the difference between the detailed synthesis procedure of the two catalysts, it is reasonable, and thus the distribution of Pd and Rh species, together with their hydrothermal aging behaviors, is schematically described in Fig. 5.

As shown in Fig. 5(a), for conventional Pd + Rh catalyst, Pd species are distributed on Al_2O_3, and Rh species are distributed on CZ, which are mainly present as oxidative PdO and reducible Rh_2O_3 species, respectively. During hydrothermal aging treatment, Pd species on Al_2O_3 is tend to agglomerate to a large extent, and meanwhile, transformation of PdO to large metallic Pd clusters is easily taken place. On the other hand, Rh species on CZ also undergoes severe deactivation in terms of self-aggregation accompanied by transformation into reduction-resistive RhO_2 clusters. However, when part of Rh species is moved to the surface of Al_2O_3 support, the hydrothermal aging behaviors of Pd and Rh species can both be modified. As seen from Fig. 5(b), partial Rh is distributed on Al_2O_3 support together with Pd species, and the residual portion of Rh is distributed on CZ component. Under this condition, the co-impregnated Rh species may act as an auxiliary for the Pd catalyst, that is, the self-aggregation of noble metal species on Al_2O_3 support during hydrothermal aging treatment can be well retarded due to the diffusion barrier effect, and Rh species on CZ component also undergoes agglomeration to a lesser extent on account of the lower concentration of Rh species on CZ. Furthermore, owing to the synergistic effect of Pd-Rh interaction, more Pd and Rh species could be maintained at more active PdO and Rh_2O_3 states, which is consequently advantageous to the catalytic performance of (PdRh + Rh)a.

3.4. XPS analysis results

The surface elemental composition derived from XPS measurement results is compiled in Table 2, wherein it is found that due to the considerably low loading contents of Pd and Rh species, the distinction between Pd + Rh and PdRh + Rh is negligible. Notwithstanding, the variation of the surface concentrations of Pd and Rh upon hydrothermal aging treatment can provide us some information. As can be seen in Table 2, after hydrothermal aging treatment, the surface concentration of Pd becomes much lower, which is ascribed to the particle agglomeration during aging process.

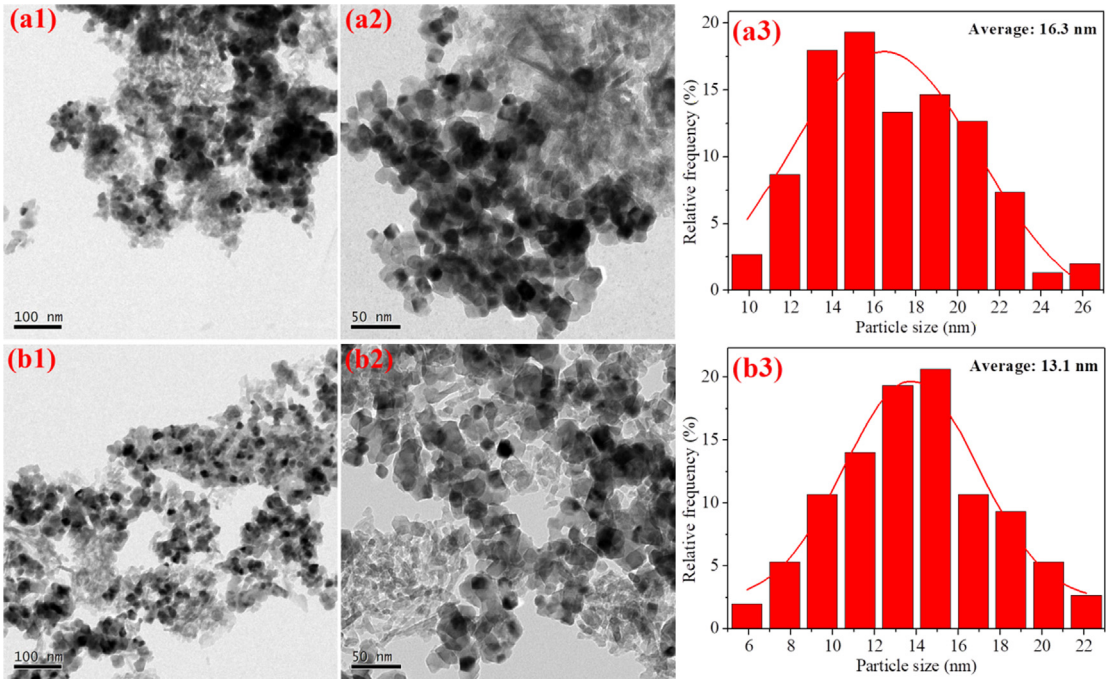

Fig. 3 TEM images and the corresponding particle size distributions of (Pd + Rh)a (a1-a3) and (PdRh + Rh)a (b1-b3).

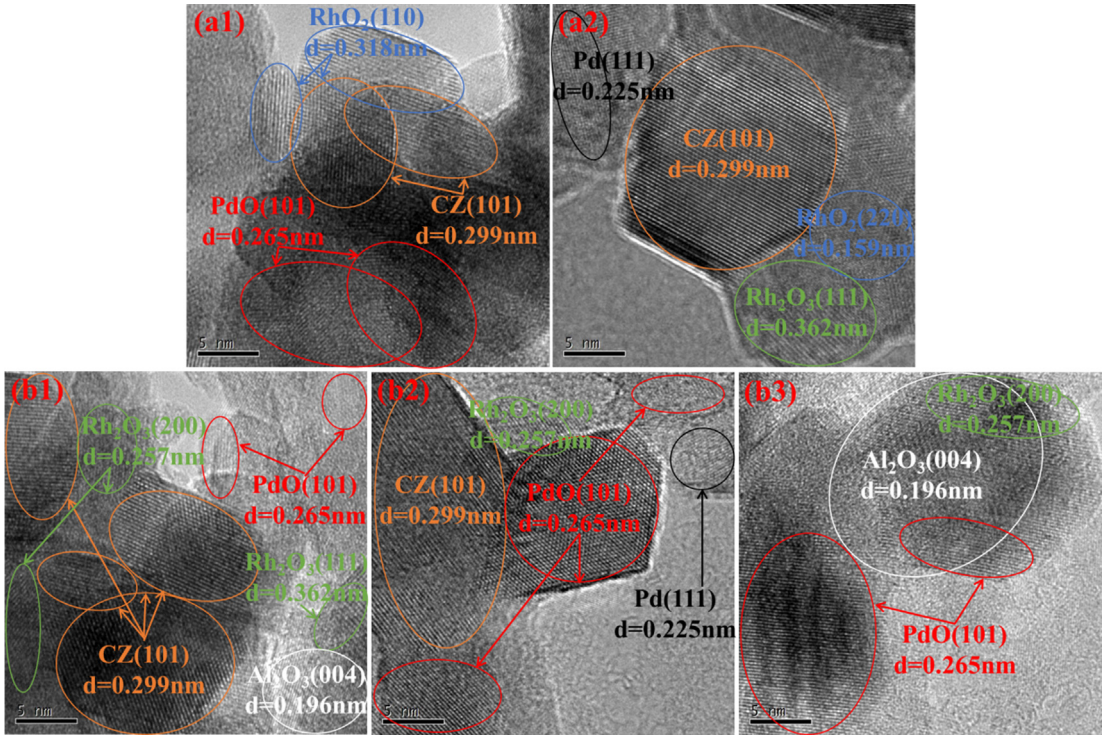

Fig. 4 HRTEM images of (Pd + Rh)a (a1, a2) and (PdRh + Rh)a (b1, b2, b3).

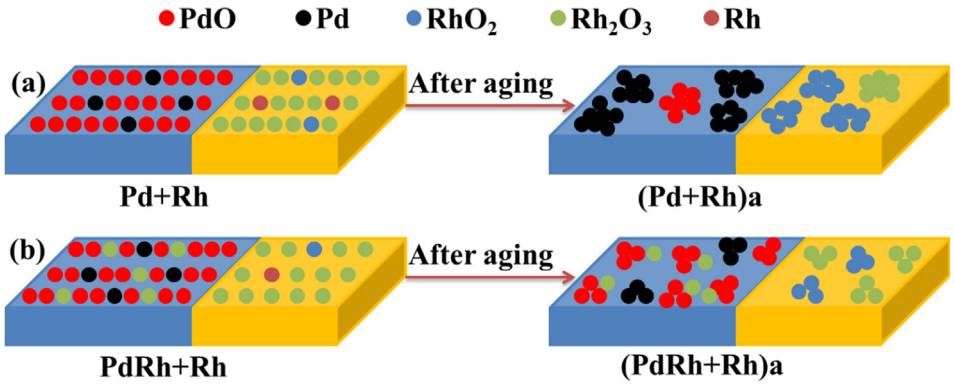

Fig. 5 Schematic illustration describing the distribution of Pd and Rh species and their hydrothermal aging behaviors.

However, the surface concentration of Rh conversely increases upon aging treatment, which is due to that besides particle agglomeration, Rh species has larger tendency to stay at the outer surface of the catalysts.

In addition, besides the surface composition, detailed analysis of the XPS spectra can also provide us some information about the chemical state of the surface elements. Fig. 6 displays the curve fitting results of the Pd 3d, Rh 3d and O 1 s

Table 2 Surface elemental information derived from the XPS analysis results.

Samples	Relative amount (%)						Pd (eV)	Rh (eV)	O_β/O (%)
	Pd	Rh	Ce	Zr	Al	O			
Pd + Rh	0.09	0.10	0.64	2.33	33.17	63.67	336.7	308.8	71.97
PdRh + Rh	0.10	0.11	0.84	2.94	32.75	63.26	336.8	308.9	73.05
(Pd + Rh)a	0.03	0.16	0.99	3.37	31.28	64.17	336.3	310.2	64.35
(PdRh + Rh)a	0.04	0.17	0.95	3.20	31.51	64.13	336.7	309.7	71.42

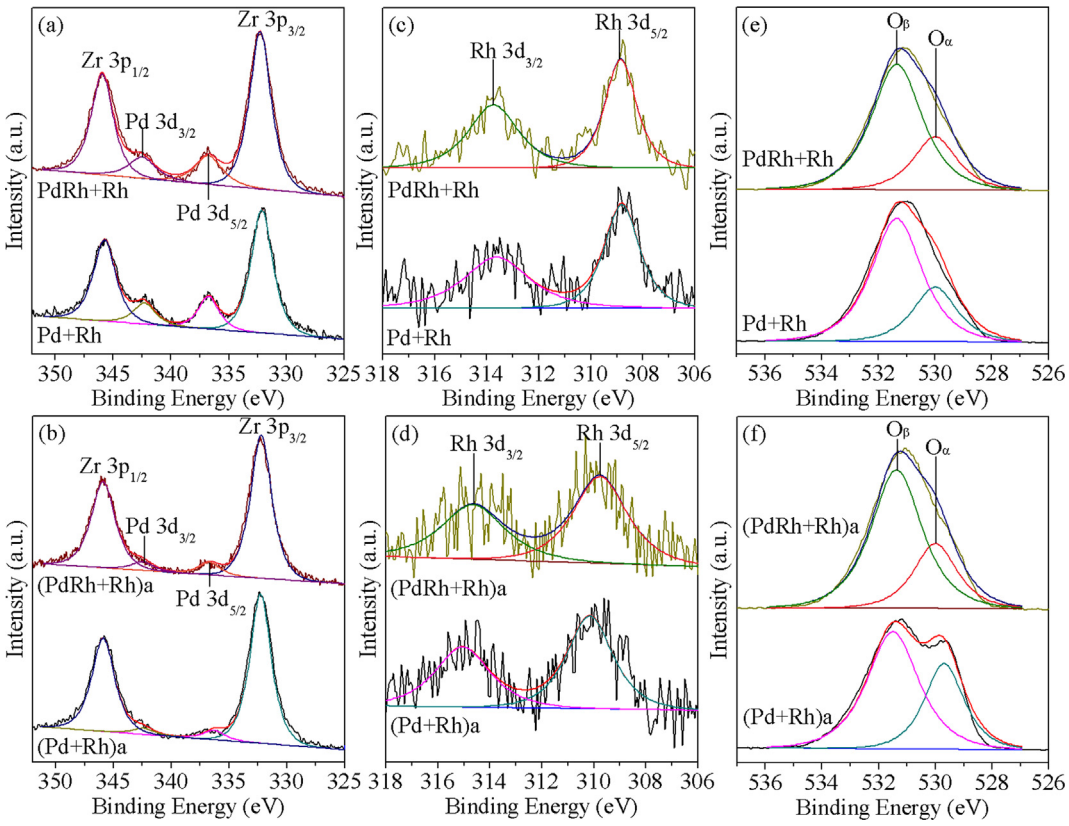

Fig. 6 XPS spectra of Pd 3d, Rh 3d and O 1 s core levels for the fresh (a, c, e) and aged (b, d, f) catalysts.

XPS spectra. The binding energies of Pd $3d_{5/2}$ and Rh $3d_{5/2}$ are also listed in Table 2. As found therein, the values for the two fresh catalysts are close to each other, which are about 336.7 eV and 308.8 eV for Pd and Rh, respectively, indicating that Pd species are mainly in oxidative Pd^{2+} state and Rh species are mainly present as reducible Rh^{3+} state (Heo et al., 2012; Shen et al., 2009; Weng et al., 2011; Wu et al., 2004). After hydrothermal aging treatment, the XPS peak of Pd for (Pd + Rh)a shifts towards lower binding energy, which coincides with the XRD and HRTEM observations that reduction of PdO to metallic Pd species has happened. Whereas for (PdRh + Rh)a, the position of Pd XPS peak is almost the same with fresh PdRh + Rh, meaning that the oxidative state of Pd^{2+} is well protected because of the favorable Pd-Rh interaction, which agrees well with the Raman and HRTEM results. When it comes to Rh species, similar phenomenon is observed. Rh species in (Pd + Rh)a experiences transformation to Rh^{4+} state to a large extent, while the Rh XPS peak stays at relatively lower binding energy for (PdRh + Rh)a, implying that more Rh^{3+} species is maintained.

In addition, two types of surface oxygen species are recognized from Fig. 6(e, f), the peak at lower binding energy (O_α) is ascribed to lattice oxygen, and the other one located at higher binding energy (O_β) is attributed to surface adsorbed oxygen species, oxygen vacancies or hydroxyl groups (Santos et al., 2010; Sellick et al., 2013). It is generally accepted that oxygen species in O_β region has higher mobility than lattice oxygen, thus the relative concentration of O_β is important to the catalytic reaction process (Li et al., 2017). As displayed in Table 2, the two fresh catalysts own similar proportion of O_β species, while after hydrothermal aging treatment, the value for (PdRh + Rh)a is much larger than that for (Pd + Rh)a, indicating that oxygen species on the surface of (PdRh + Rh)a may be more active, which could consequently well contribute to its enhanced catalytic performance.

3.5. CO adsorption experimental results

The CO adsorption experimental results are illustrated in Fig. 7. For the purpose of better analysis, the CO-FTIR spectra of Pd/A and Rh/CZ both before and after aging treatment are also included in Fig. 7. From Fig. 7(a), it is observed that for Pd/A, the linearly adsorbed CO species produces an adsorption band at 2056 cm^{-1}, and the peak for bridged or three-fold CO adsorption species is centered at 1880 cm^{-1} (Lin et al., 2015). On the other hand, three CO adsorption peaks are observed for Rh/CZ, among which the peak at 2063 cm^{-1} is originated from the linearly-bonded CO species, and the other two peaks at 2084 and 2013 cm^{-1} are attributed to asymmetric and symmetric stretching vibration modes of germinal dicarbonyl species, respectively (Machida et al., 2015; Yang and Garland, 1957). Moreover, it is claimed by previous researchers that the two bands at 2084 and 2013 cm^{-1} should have equal intensity regardless of the coverage (Yang and Garland, 1957). Accordingly, the CO adsorption peaks of the two Pd-Rh bimetallic catalysts are identified. As can be seen from Fig. 7(a), the CO adsorption peaks of Rh species for the two fresh catalysts are similar with each other, implying their similar Rh dispersion state. While

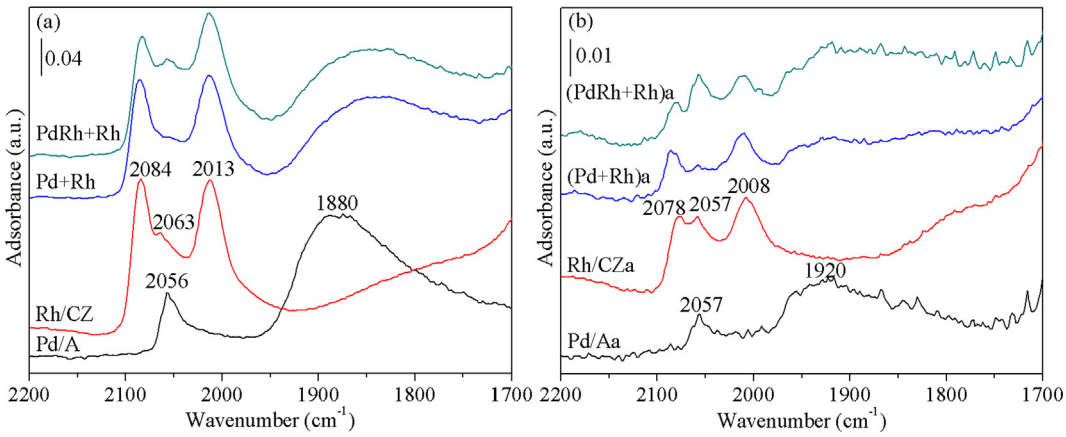

Fig. 7 CO-FTIR spectra of the fresh (a) and aged (b) catalysts. For comparison's sake, legends represent the relative intensities of Y-axes are plotted.

PdRh + Rh shows a stronger band at ca. 2056 cm^{-1}, indicating that Pd species on the surface of PdRh + Rh are better dispersed.

Owing to the particle agglomeration during hydrothermal aging treatment, the CO adsorption peaks of the aged samples become much weaker, implying that the dispersion of Pd and Rh species is declined to a large extent. Nevertheless, it can be found from Fig. 7(b) that the intensities of the peaks at ca. 2057 and 1920 cm^{-1} for (PdRh + Rh)a are much higher than those for (Pd + Rh)a, which is indicative of the higher dispersion of Pd species for (PdRh + Rh)a, and is in line with the TEM observation results.

3.6. H_2-TPR investigation

H_2-TPR profiles of the fresh and aged Pd-Rh bimetallic catalysts, together with those of the reference samples Pd/A and Rh/CZ, are depicted in Fig. 8. As displayed therein, in the experimental temperature region, Pd/A shows a single reduction peak at 90 °C, which is ascribed to the reduction of PdO species. With respect to Rh/CZ, two reduction peaks are observed, the intense one located at around 132 °C is assigned to the reduction of surface Rh_2O_3 species, and the other weaker peak centered at 280 °C is generated by the reduction of surface Ce species, while the reduction temperature is much lower than that for bare CZ support (as shown in the inset of Fig. 8(a), the reduction of surface Ce species begins at about 350 °C), implying that the reduction of Ce species is promoted by Rh species on account of the H_2 spill-over effect from Rh to the support (Heo et al., 2012). Accordingly, the three reduction peaks in the profiles of the Pd-Rh bimetallic catalysts can be categorized into the reduction of PdO, surface Rh_2O_3 species, and surface Ce species, respectively. In addition, a comparison between the H_2-TPR profiles of PdRh + Rh and Pd + Rh tells us that by co-impregnating partial Rh with Pd, the reduction of PdO species for PdRh + Rh is somewhat promoted due to the synergistic effect between Pd and Rh. And on the other hand, the intensity of the reduction peak for surface Rh_2O_3 species is slightly lower, which is probably due to the lower concentration of Rh on the surface of CZ component.

After hydrothermal aging treatment, as shown in Fig. 8(b), the reduction characteristic of Pd/Aa resembles that of fresh Pd/A, while for Rh/CZa, great difference is observed. Only a broad reduction peak centered at 185 °C is found for Rh/CZa, which is caused by the aggregation and diffusion of Rh species into the support (Heo et al., 2012). When it comes to

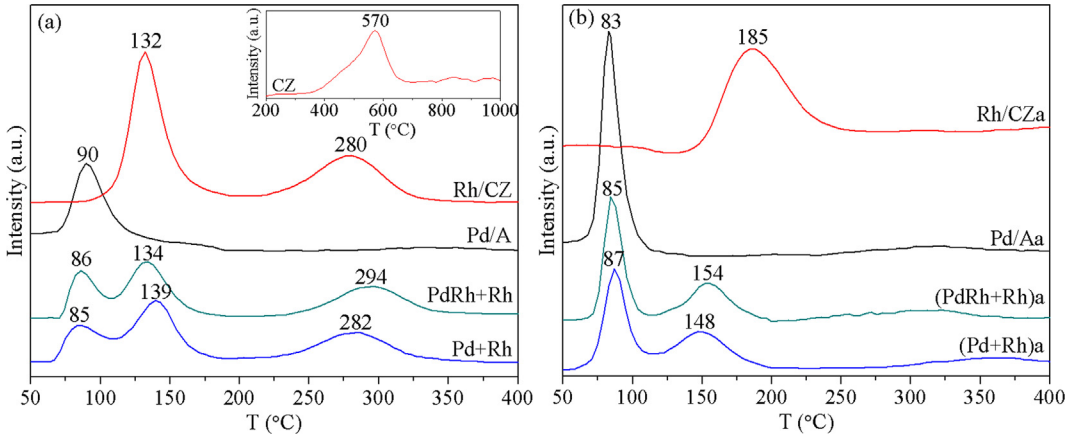

Fig. 8 H_2-TPR profiles of the fresh (a) and aged (b) catalysts, the inset is the H_2-TPR profile of the CZ support.

the Pd-Rh bimetallic catalysts, besides the reduction of PdO that occurs at around 85 °C, the reduction of Rh species appears at around 150 °C, which seems to be promoted compared with that of single Rh/CZ. It is also noted from Fig. 8 (b) that while the reduction of the two aged catalysts occurs at similar temperatures, the reduction peak areas of (PdRh + Rh)a are larger than those of (Pd + Rh)a, demonstrating the presence of more reducible species in (PdRh + Rh)a, which is advantageous to the catalytic reaction process.

3.7. Catalytic performance evaluation results

Fig. 9 displays the catalytic performance evaluation results in terms of catalytic conversions of CO, HC and NO as a function of temperature (light-off performance) as well as time (air-to-fuel ratio fluctuation performance). In addition, the turnover frequency (TOF) values of the fresh and aged catalysts at 300 and 360 °C are summarized in Table 3. From Fig. 9(a-c), it is observed that the two fresh catalysts exhibit similar catalytic conversion efficiency of CO, HC and NO, but after hydrothermal aging treatment, the modified catalyst (PdRh + Rh)a behaves much better, the catalytic conversions of which are higher than those of (Pd + Rh)a over most of the experimental temperature range. On the other hand, from the viewpoint of turnover frequency (TOF), it is observed from Table 3 that both at 300 and 360 °C, the TOF values of the two fresh catalysts are similar, while after hydrothermal aging treatment, the values of (PdRh + Rh)a are larger than those of (Pd + Rh)a, which again confirms the better catalytic activity of (PdRh + Rh)a. Moreover, it can be found from Fig. 9(d-f) that the variation of catalytic conversions of CO, HC and NO over time is similar with each other for the two fresh catalysts. Whereas for the aged catalysts, (PdRh + Rh)a still behaves better, the conversions of CO, HC and NO are maintained at relatively higher levels and show fluctuation to lesser extents, which represent its higher conversion efficiency. Combined with the above characterization results of the catalysts, the following reasons are considered responsible for the superior catalytic performance of (PdRh + Rh)a: 1) When part of Rh is co-impregnated with Pd on Al_2O_3 support, Rh may act as a diffusion barrier to suppress the agglomeration of Pd species, and the dispersion of Rh species is modified as well, thus after hydrothermal aging treatment, higher dispersion of Pd and Rh species can be achieved for (PdRh + Rh)a, which represents larger amount of catalytic active sites compared with (Pd + Rh)a, and is consequently advantageous to the catalytic performance. 2) For supported noble metal catalysts, besides the dispersion of noble metal species, the oxidation state is equally important for the catalytic conversions. It is considered that for (PdRh + Rh)a, the favorable interaction between Pd and Rh has the ability to maintain more Pd and Rh species at PdO and Rh_2O_3 states, which are more active during the catalytic reaction process. 3) The higher oxygen mobility on the surface of (PdRh + Rh)a can also account for its superior catalytic performance.

4. Conclusions

In this work, an advanced Pd-Rh bimetallic catalyst PdRh + Rh was synthesized by adjusting the synthesis procedure of conventional Pd + Rh catalyst composed of Al_2O_3-

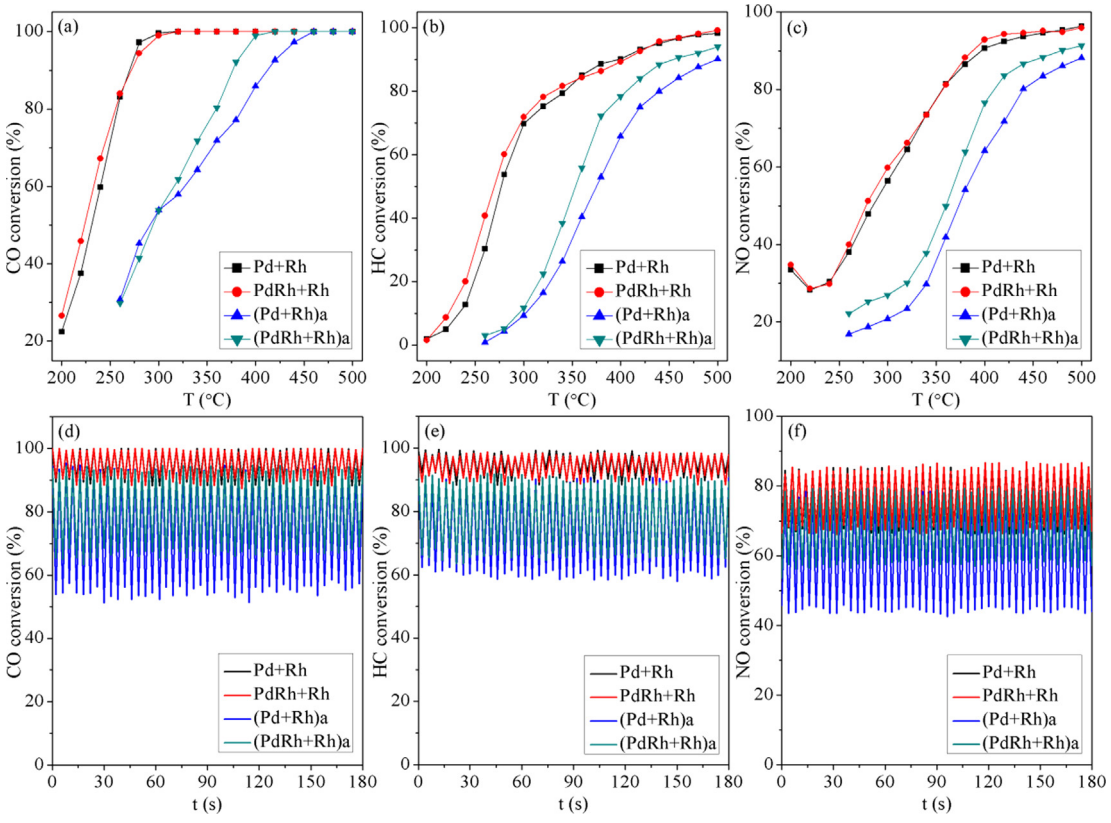

Fig. 9 Catalytic conversions of CO, HC and NO as function of temperature (a-c) and time (d-f).

Table 3 The turnover frequency (TOF) values of the fresh and aged catalysts at 300 and 360 °C.

Samples	300 °C			360 °C		
	CO (s^{-1})	HC (s^{-1})	NO (s^{-1})	CO (s^{-1})	HC (s^{-1})	NO (s^{-1})
Pd + Rh	0.0789	0.00397	0.0121	0.0717	0.00438	0.0159
PdRh + Rh	0.0784	0.00409	0.0129	0.0717	0.00435	0.0158
(Pd + Rh)a	0.0393	0.000487	0.00411	0.0676	0.00211	0.00828
(PdRh + Rh)a	0.0392	0.000609	0.00532	0.0729	0.00292	0.00988

supported Pd and CZ-supported Rh. That was, a portion of Rh was co-impregnated with Pd on Al_2O_3, and the residual portion of Rh was still supported on CZ. Under this condition, the co-impregnated Rh may act as a diffusion barrier to suppress the agglomeration of Pd species upon hydrothermal aging treatment. Meanwhile, on account of the synergistic effect of Pd-Rh interaction, more Pd and Rh species are stayed at PdO and Rh_2O_3 states, which are catalytically more active. These phenomena, together with the higher mobility of surface oxygen species in (PdRh + Rh)a, contribute well to its superior catalytic performance for conversions of CO, HC and NO.

On the other hand, the findings in this work could provide us some inspiration to further optimize the Pd-Rh bimetallic catalyst. For example, it is reasonably inferred that the catalytic performance of PdRh + Rh may be greatly influenced by the ratio between the amount of Rh co-impregnated with Pd and that supported on CZ. Moreover, co-impregnating a portion of Pd with Rh on CZ support, and the combination of simultaneously adjusting the distribution of both Pd and Rh, are all possible to improve the catalytic performance of the Pd-Rh bimetallic catalyst.

Declaration of Competing Interest

The authors declare that they have no known competing financial interests or personal relationships that could have appeared to influence the work reported in this paper.

Acknowledgements

This work was financially supported by the Natural Science Foundation, China of Guangxi (Grant No. 2020GXNSFBA297029).

References

Bharali, P., Saikia, P., Reddy, B.M., 2012. Large-scale synthesis of ceria-based nano-oxides with high CO oxidation activity. Catal. Sci. Technol. 2, 931–933.

Cao, Y., Ran, R., Wu, X.D., Zhao, B.H., Wan, J., Weng, D., 2013. Comparative study of ageing condition effects on $Pd/Ce_{0.5}Zr_{0.5}O_2$ and Pd/Al_2O_3 catalysts: Catalytic activity, palladium nanoparticle structure and Pd-support interaction. Appl. Catal. A: Gen. 457, 52–61.

Cao, Y., Ran, R., Wu, X.D., Zhao, B.H., Weng, D., 2017. Improved activity and durability of Rh-based three-way catalyst under diverse aging atmospheres by ZrO_2 support. J. Environ. Sci. 52, 197–203.

Dong, Q., Yin, S., Guo, C.S., Sato, T., 2012. $Ce_{0.5}Zr_{0.4}Sn_{0.1}O_2/Al_2O_3$ catalysts with enhanced oxygen storage capacity and high CO oxidation activity. Catal. Sci. Technol. 2, 2521–2524.

Fang, R.M., Cui, Y.J., Chen, S.J., Shang, H.Y., Shi, Z.H., Gong, M. C., Chen, Y.Q., 2015. A highly efficient Rh-modified Pd/Al_2O_3 close-coupled catalyst. Chin. J. Catal. 36, 229–236.

Goto, H., Komata, K., Minami, S., 2014. Impact of Pd-Rh interaction on the performance of three-way catalysts. SAE Technical Paper. 2014–01-1503.

Graham, G.W., Jen, H.-W., Chun, W., McCabe, R.W., 1999. High-temperature-aging-induced encapsulation of metal particles by support materials: comparative results for Pt, Pd, and Rh on cerium-zirconium mixed oxides. J. Catal. 182, 228–233.

Graham, G.W., O'Neill, A.E., Uy, D., Weber, W.H., Sun, H., Pan, X. Q., 2002. Observation of strained PdO in an aged Pd/ceria-zirconia catalyst. Catal. Lett. 79, 99–105.

Heo, I., Yoon, D.Y., Cho, B.K., Nam, I., Choung, J.W., Yoo, S., 2012. Activity and thermal stability of Rh-based catalytic system for an advanced modern TWC. Appl. Catal. B: Environ. 121–122, 75–87.

Iglesias-Juez, A., Martínez-Arias, A., Fernández-García, M., 2004. Metal-promoter interface in $Pd/(Ce, Zr)O_x/Al_2O_3$ catalysts: effect of thermal aging. J. Catal. 221, 148–161.

Kang, S.B., Han, S.J., Nam, I., Cho, B.K., Kim, C.H., Oh, S.H., 2014. Detailed reaction kinetics for double-layered Pd/Rh bimetallic TWC monolith catalyst. Chem. Eng. J. 241, 273–287.

Kang, S.B., Nam, I., Cho, B.K., Kim, C.H., Oh, S.H., 2015. Kinetic model for modern double-layered Pd/Rh TWC as a function of metal loadings and mileage. Chem. Eng. J. 278, 328–338.

Kašpar, J., Fornasiero, P., Hickey, N., 2003. Automotive catalytic converters: current status and some perspectives. Catal. Today 77, 419–449.

Lan, L., Chen, S.H., Li, H.M., Li, H.M., Wu, W.X., Deng, J., Chen, Y.Q., 2018a. Controllable synthesis of zone-distributed Pd over CeO_2-ZrO_2/Al_2O_3 as advanced three-way catalyst. J. Ind. Eng. Chem. 58, 246–257.

Lan, L., Yan, C.Y., Chen, S.H., Li, H.M., Li, D.C., Wang, J.F., Cheng, Y.X., Chen, Y.Q., 2018b. Designed synthesis of semi-embedded Pd over CeO_2-ZrO_2/Al_2O_3 as advanced three-way catalyst. J. Taiwan Inst. Chem. Eng. 85, 98–105.

Lang, W., Laing, P., Cheng, Y., Hubbard, C., Harold, M.P., 2017. Co-oxidation of CO and propylene on Pd/CeO_2-ZrO_2 and Pd/Al_2O_3 monolith catalysts: A light-off, kinetics, and mechanistic study. Appl. Catal. B: Environ. 218, 430–442.

Li, H.C., Li, K.Z., Zhu, X., Du, Y.P., Wei, Y.G., Zhai, K., Wang, H., 2017. Synthesis of mesoporous $Pr_xZr_{1-x}O_{2-\delta}$ solid solution with high thermal stability for catalytic soot oxidation. J. Ind. Eng. Chem. 54, 126–136.

Lin, S.Y., Yang, L.Y., Yang, X., Zhou, R.X., 2014. Redox properties and metal-support interaction of $Pd/Ce_{0.67}Zr_{0.33}O_2$-Al_2O_3 catalyst for CO, HC and NO_x elimination. Appl. Surf. Sci. 305, 642–649.

Lin, S.Y., Yang, X., Yang, L.Y., Zhou, R.X., 2015. Three-way catalytic performance of $Pd/Ce_{0.67}Zr_{0.33}O_2$-Al_2O_3 catalysts: Role of the different Pd precursors. Appl. Surf. Sci. 327, 335–343.

López Granados, M., Cabello Galisteo, F.C., Mariscal, R., Alifanti, M., Gurbani, A., Fierro, J.L.G., Fernández-Ruíz, R., 2006. Modification of a three-way catalyst washcoat by aging: A study along the longitudinal axis. Appl. Surf. Sci. 252, 8442–8450.

Machida, M., Minami, S., Hinokuma, S., Yoshida, H., Nagao, Y., Sato, T., Nakahara, Y., 2015. Unusual redox behavior of Rh/$AlPO_4$ and its impact on three-way catalysis. J. Phys. Chem. C 119, 373–380.

Majumdar, S.S., Pihl, J.A., 2020. Impact of selected high-performance fuel blends on three-way catalyst light off under synthetic spark-ignition engine-exhaust conditions. Energ. Fuel. 34, 12900–12910.

Panahi-Kalamuei, M., Alizadeh, S., Mousavi-Kamazani, M., Salavati-Niasari, M., 2015. Synthesis and characterization of CeO_2 nanoparticles via hydrothermal route. J. Ind. Eng. Chem. 21, 1301–1305.

Papavasiliou, A., Tsetsekou, A., Matsouka, V., Konsolakis, M., Yentekakis, I.V., 2010. An investigation of the role of Zr and La dopants into $Ce_{1-x-y}Zr_xLa_yO_\delta$ enriched γ-Al_2O_3 TWC washcoats. Appl. Catal. A: Gen. 382, 73–84.

Polvinen, R., Vippola, M., Valden, M., Lepistö, T., Suopanki, A., Härkönen, M., 2004. The effect of Pt-Rh synergism on the thermal stability of rhodium oxide on pure alumina and Ce-ZrO_2-modified alumina-supported catalysts. J. Catal. 226, 372–381.

Rassoul, M., Gaillard, F., Garbowski, E., Primet, M., 2001. Synthesis and characterisation of bimetallic Pd-Rh/alumina combustion catalysts. J. Catal. 203, 232–241.

Santos, V.P., Pereira, M.F.R., Órfão, J.J.M., Figueiredo, J.L., 2010. The role of lattice oxygen on the activity of manganese oxides towards the oxidation of volatile organic compounds. Appl. Catal. B: Environ. 99, 353–363.

Sellick, D.R., Aranda, A., García, T., López, J.M., Solsona, B., Mastral, A.M., Morgan, D.J., Carley, A.F., Taylor, S.H., 2013. Influence of the preparation method on the activity of ceria zirconia mixed oxides for naphthalene total oxidation. Appl. Catal. B: Environ. 132–133, 98–106.

Shen, M.Q., Yang, M., Wang, J., Wen, J., Zhao, M.W., Wang, W.L., 2009. Pd/support interface-promoted Pd-$Ce_{0.7}Zr_{0.3}O_2$-Al_2O_3 automobile three-way catalysts: Studying the dynamic oxygen storage capacity and CO, C_3H_8, and NO conversion. J. Phys. Chem. C 113, 3212–3221.

Soloviev, S.O., Kyriienko, P.I., Popovych, N.O., 2012. Effect of CeO_2 and Al_2O_3 on the activity of Pd/Co_3O_4/cordierite catalyst in the three-way catalysis reactions (CO/NO/C_nH_m). J. Environ. Sci. 24, 1327–1333.

Vedyagin, A.A., Gavrilov, M.S., Volodin, A.M., Stoyanovskii, V.O., Slavinskaya, E.M., Mishakov, I.V., Shubin, Y.V., 2013. Catalytic purification of exhaust gases over Pd-Rh alloy catalysts. Top. Catal. 56, 1008–1014.

Vedyagin, A.A., Volodin, A.M., Kenzhin, R.M., Stoyanovskii, V.O., Shubin, Y.V., Plyusnin, P.E., Mishakov, I.V., 2017. Effect of metal-metal and metal-support interaction on activity and stability of Pd-Rh/alumina in CO oxidation. Catal. Today 293–294, 73–81.

Vedyagin, A.A., Stoyanovskii, V.O., Plyusnin, P.E., Shubin, Y.V., Slavinskaya, E.M., Mishakov, I.V., 2018. Effect of metal ratio in alumina-supported Pd-Rh nanoalloys on its performance in three way catalysis. J. Alloy. Compd. 749, 155–162.

Weng, X.L., Zhang, J.Y., Wu, Z.B., Liu, Y., Wang, H.Q., Darr, J.A., 2011. Continuous syntheses of highly dispersed composite nanocatalysts via simultaneous co-precipitation in supercritical water. Appl. Catal. B: Environ. 103, 453–461.

Wu, X.D., Xu, L.H., Weng, D., 2004. The thermal stability and catalytic performance of Ce-Zr promoted Rh-Pd/γ-Al_2O_3 automotive catalysts. Appl. Surf. Sci. 221, 375–383.

Yang, A.C., Garland, C.W., 1957. Infrared studies of carbon monoxide chemisorbed on rhodium. J. Phys. Chem. 61, 1504–1512.

Zhan, Z.C., Song, L.Y., Liu, X.J., Jiao, J., Li, J.Z., He, H., 2014. Effects of synthesis methods on the performance of Pt + Rh/$Ce_{0.6}Zr_{0.4}O_2$ three-way catalysts. J. Environ. Sci. 26, 683–693.